ANNALS OF GEOPHYSICS, 69, 5, NS550, 2026; doi:10.4401/ag-9571
OPEN ACCESS

Seismic Microzonation and Geotechnical Evaluation for Urban Extension in Tiznit, Morocco

Ismaail Khadrouf[*,1], Fadoua Cherki[2], Nadia Mhammdi[2], Ouafa El Hammoumi[1], Najib El Goumi[3], Abdessamad El Atillah[4], Youssef Raddi[5]

(1) Hassan II University of Casablanca, Faculty of Sciences Ben M'sick, Laboratory of Geosciences, Geomatics and Environment, Morocco
(2) Mohammed V University in Rabat, Scientific Institute, GEOPAC Research Center, Geophysics and Natural Hazards Laboratory, Morocco
(3) University of Cadi Ayyad, Faculty of Science and Technology, Earth Sciences Department, Georesources Laboratory, Marrakech, Morocco
(4) Ibnou Zohr University, Faculty of Languages Arts and Human Sciences, Department of Geography and Planning Spaces Societies Environment, Planning and Development Laboratory, Ait Melloul, Morocco
(5) Mohammed V University, Faculty of Sciences Agdal, Department of Earth Sciences, Rabat Agdal, Morocco

Article history: received April 8, 2026; accepted July 10, 2026

Abstract

Following the 2023 Al Haouz earthquake, seismic site characterization has become a critical priority for improving seismic risk assessment and guiding safer urban development. In this context, Tiznit, located in southwestern Morocco and currently undergoing rapid urban expansion, requires reliable seismic and geotechnical characterization to support informed land-use planning and appropriate foundation design. This study presents an integrated microzonation-oriented investigation based on Horizontal-to-Vertical Spectral Ratio (HVSR), Multichannel Analysis of Surface Waves (MASW), Seismic Refraction Tomography (SRT), Dynamic Penetration Testing (DPT), boreholes, and geological observations. The objective was to evaluate the spatial variability of site response and near-surface ground conditions, and to identify sectors requiring particular engineering attention. The results show that the study area is dominated by generally stiff ground conditions, with shallow competent substratum over large parts of the site. HVSR measurements reveal mostly flat to weakly peaked curves, indicating limited impedance contrast in many sectors, whereas localized peaked or multi-peaked responses reflect more heterogeneous superficial deposits. The MASW results indicate predominantly Eurocode 8 class B conditions, with limited class A sectors and localized softer zones. SRT and DPT data confirm a generally shallow geotechnical and seismic bedrock, while the mapped weaker corridor sectors exhibit lower stiffness and reduced serviceability capacity. These findings suggest that Tiznit does not behave as a uniformly amplification-prone sedimentary basin, but rather as a mostly competent site interrupted by discrete zones of geotechnical and seismic sensitivity. The study therefore provides a practical basis for seismic microzonation, foundation assessment, and more rational urban planning in the Tiznit urban extension area.

Keywords: Seismic microzonation; Site characterization; HVSR; MASW; Seismic bedrock; V_{s30}; Tiznit; Morocco

1. Introduction

The Mw 6.9 Al Haouz earthquake of 2023 has exposed significant limitations in Morocco's seismic framework, underscoring the urgent need for comprehensive seismic and geotechnical assessments. Such evaluations are particularly crucial in zones of urban expansion, such as Tiznit. This area is located approximately 250 km from the 23 Al Haouz epicenter and lies between the two major active orogenic belts of the High Atlas and Anti-Atlas (Khadrouf et al., 2024). More than 320,000 people were reported affected, and the event caused a death toll exceeding 2,900 with prolonged disruption to housing and basic services, highlighting systemic exposure of vulnerable settlements and construction typologies in mountainous and peri-urban areas (Nouayti et al., 2024).

Beyond the immediate humanitarian consequences, this event reaffirmed a central geotechnical earthquake engineering lesson: damage patterns are often governed by site response as much as by source characteristics. In rapidly growing Moroccan towns, expansion commonly occurs over laterally variable Quaternary deposits, weathered bedrock, and mixed alluvial-colluvial terrains where impedance contrasts and basin geometry can amplify shaking, shift frequency content, and intensify ground deformation demands. These effects directly control foundation performance, slope and retaining stability, and the resilience of lifelines that frequently cross heterogeneous ground conditions.

Morocco's historical record further underscores the outsized consequences of unfavorable site conditions coupled with vulnerable construction. The 1960 Agadir earthquake (Mw 5.9) caused an estimated 12,000-15,000 fatalities despite its moderate magnitude, illustrating how shallow shaking, local amplification, and structural fragility can combine to produce catastrophic outcomes (Khadrouf et al., 2024). More recent damaging events across the Atlas and Rif domains reiterate that national-scale hazard zonation alone does not resolve the local drivers of damage, particularly where seismic demand is controlled by near-surface stratigraphy and stiffness contrasts at the scale of neighborhoods (El Hilali et al., 2023).

Regulatory practice reflects this tension. The Moroccan seismic code framework prescribes normalized design spectra with site coefficients tied to site categories (S1-S5) and recommends adopting a default site class when ground information is insufficient (RPS, 2011). While operationally convenient, default classification can be non-conservative in urban-expansion settings where shallow soft layers, variable sediment thickness, or special ground conditions govern short-period demand and increase susceptibility to settlement, instability, and service disruption. This motivates site-specific, evidence-based characterization that produces design-relevant inputs rather than solely descriptive indicators.

Recent Moroccan case studies have advanced cost-effective approaches for quantifying site effects, particularly through ambient vibration and surface-wave methods (Chaaraoui et al., 2022; El Hilali et al., 2023; Khadrouf et al., 2024; Essaied et al., 2025; Lamine et al., 2026; Khadrouf et al., 2026). HVSR has become a standard tool for dense spatial sampling and resonance mapping (Nakamura, 1989), with subsequent work clarifying its robustness for fundamental frequency estimation while cautioning that amplitude interpretation requires careful wavefield and impedance considerations (Bonnefoy-Claudet et al., 2006). Contemporary surface-wave practice, supported by rigorous acquisition and inversion guidelines, enables improved constraints on shallow shear-wave velocity structure and site classification (Foti et al., 2018). Importantly, integrated microzonation-oriented workflows are emerging in Morocco: in Ghabt Admin (Agadir), HVSR and MASW were combined with geotechnical investigations to support safe urban extension decisions (Khadrouf et al., 2024). In Tiznit, HVSR-based V_{s30} mapping reported values spanning approximately 254-435 m/s, implying meaningful spatial variability in expected amplification and code-relevant site classes (Cherki et al., 2025). In Taroudant, amplification factors mapped from combined observations ranged roughly from 1.68 to 2.0, explicitly linking soft terrace deposits to higher expected site amplification (Hitouri et al., 2025).

Despite these advances, two limitations continue to restrict translation into design-grade geotechnical earthquake engineering practice. First, many studies remain anchored to proxies such as f_0 and V_{S30} without systematically converting them into spectrum-consistent, engineering-ready amplification measures under defensible subsurface models. Second, the uncertainty introduced by lateral heterogeneity and non-uniqueness in inversion is seldom propagated into the design implications that govern permitting, retrofit prioritization, and land-use regulation, precisely the decisions that are most urgent in fast-growing towns such as Tiznit.

The present study addresses this gap by developing an integrated, microzonation-oriented characterization for Tiznit that leverages dense ambient-noise constraints within a framework explicitly aligned with geotechnical earthquake engineering needs. The objectives are to delineate spatially coherent site zones, reduce reliance on default code assumptions through multi-constraint ground modeling, and derive design-relevant site effect descriptors suitable for urban planning and engineering applications. The novelty lies in the direct coupling of mapped

site-response indicators to in-situ parameters, thereby strengthening the operational bridge between near-surface characterization and risk-informed urban expansion.

2. Geological and geomorphological context

Tiznit area is located on the northern fringe of the western Anti-Atlas, at the transition between the Tiznit plain – considered the southern extension of the Souss Basin – and the Lakhssas Plateau, which forms a structural bridge between the Precambrian inliers of Ifni to the west and Kerdous to the east (Wanaim et al., 2014). From a regional perspective, this sector belongs to the northern margin of the West African Craton and is characterized by a Precambrian crystalline basement overlain by a thick late Neoproterozoic to Paleozoic cover; near Tiznit, this cover includes volcano-detrital Ediacaran units, Adoudounian dolomites and limestones, Lower to Middle Cambrian carbonates and schists, and Ordovician quartzitic formations, while the surrounding lowlands are locally mantled by recent Cretaceous, Pliocene, and Quaternary deposits (Sehrt, 2014) (Fig. 1). Structurally, the Tiznit-Lakhssas domain records a post-Pan-African extensional stage that generated synsedimentary normal faults and a N-S to submeridional hemi-graben architecture, later reactivated during the Variscan compression, which produced folds, shear zones, and fault-controlled relief organization (Soulaimani and Bouabdelli, 2005). This inherited tectono-stratigraphic framework explains the present geological configuration of the Tiznit area, where carbonate plateaus, folded Paleozoic ridges, fault corridors, and Quaternary plains are closely associated in a strongly structured western Anti-Atlas landscape.

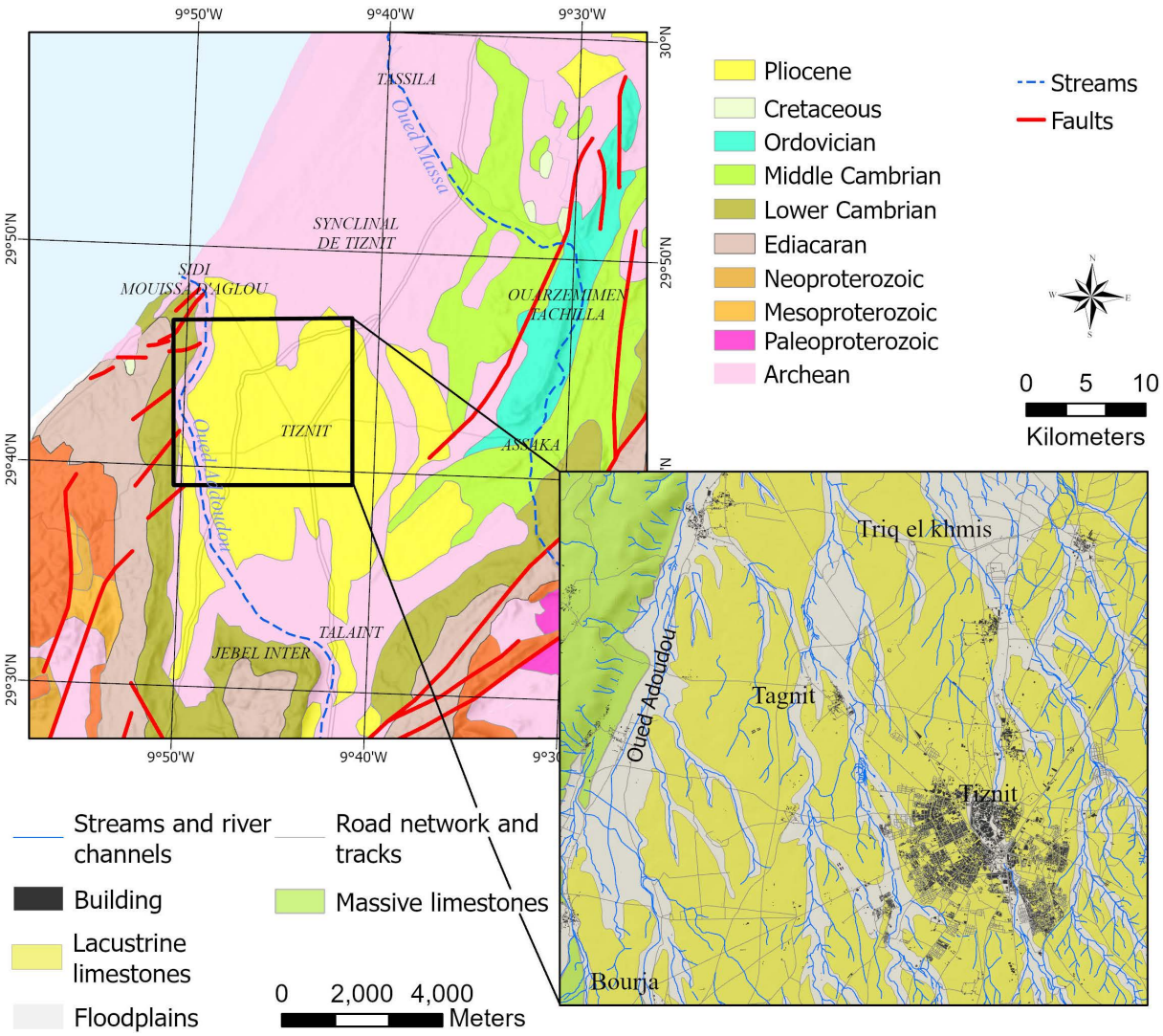

Figure 1. Geological and structural map of the Tiznit area, Western Anti-Atlas, Morocco.

3. Data and Method

The methodology follows an integrated site-investigation workflow that combines passive and active seismic methods with in-situ geotechnical control to derive consistent, mappable proxies for site characterization. The investigations were arranged to cover all lithological units (Fig. 3). Ambient-noise HVSR measurements were acquired across the study area and processed to extract the fundamental resonance frequency (f_0) and peak amplification (A_0), which provide first-order constraints on impedance contrasts and potential site effects. In parallel, MASW and SRT profiles were carried out to retrieve shear and compressional wave velocity models (V_p and V_s), from which V_{s30} (and the corresponding EC8 class) and the seismic bedrock geometry were estimated and cross-checked against the HVSR indicators. Geotechnical investigations (DPT and boreholes) were used to define soil stratigraphy, to constrain the geotechnical basement depth, and to compute an equivalent serviceability bearing pressure (q_{els}) at each investigation point. Finally, all derived parameters were integrated in a GIS environment and spatially interpolated to produce the final interpretation and mapping products used for site characterization and zoning (Fig. 2).

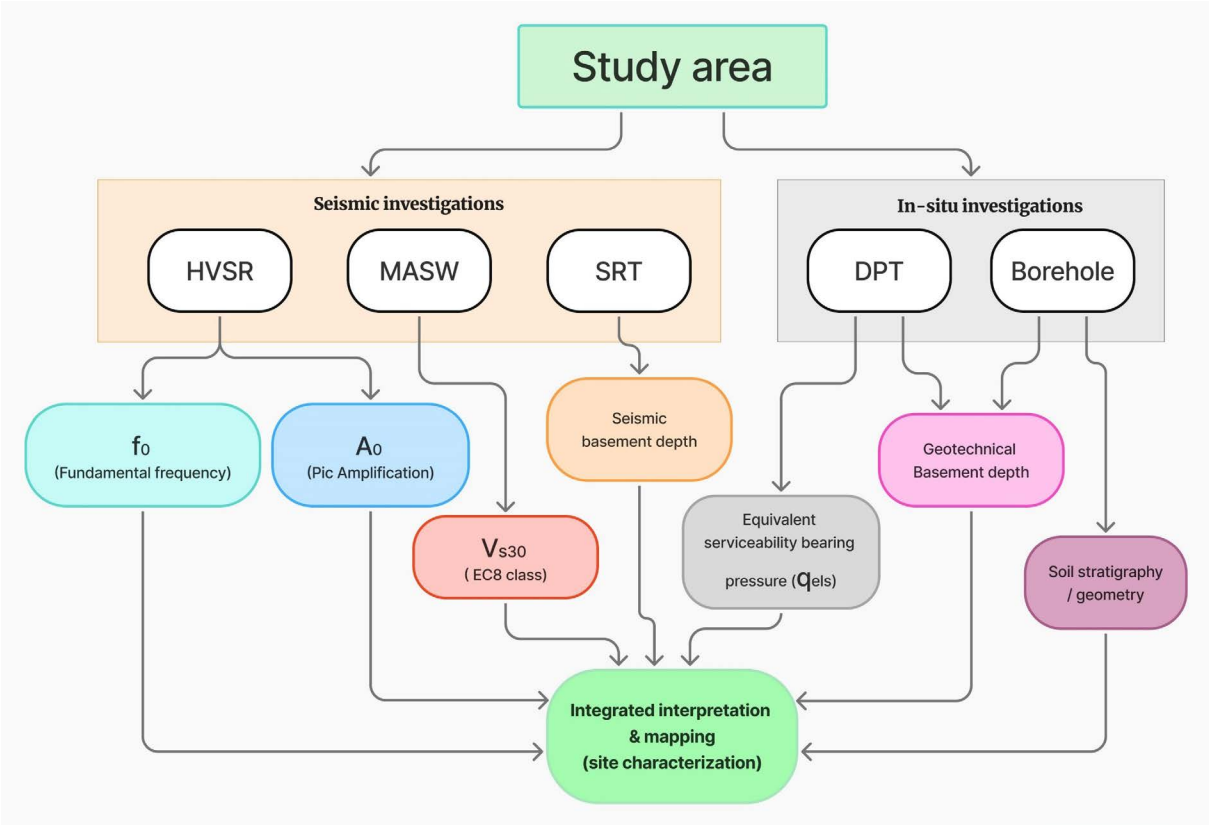

Figure 2. Flowchart illustrating the integrated geophysical and geotechnical workflow for site characterization.

3.1 HVSR

The Horizontal-to-Vertical Spectral Ratio (HVSR) technique is widely used in seismic microzonation because it is simple, cost-effective, and particularly suitable for areas of low to moderate seismicity. Originally introduced by Nogoshi and Igarashi (1970) and later formalized by Nakamura (1989), this method relies on the analysis of ambient vibrations generated by both natural and anthropogenic sources. The ratio between the horizontal and vertical spectral components is interpreted as a pseudo-transfer function, providing a robust estimate of the fundamental resonance frequency of sedimentary deposits, especially in settings characterized by subhorizontal layering and strong impedance contrasts (Bonnefoy-Claudet et al., 2006).

In the present study, ambient noise measurements were collected at 60 stations across Tiznit area using a DaqLink seismograph coupled with an LE-3D/5s MKIII triaxial geophone (Fig. 3). Each record lasted approximately 20 minutes,

with a sampling frequency of 125 Hz, while station locations were determined using GPS. Data processing was performed in Geopsy (Wathelet et al., 2020), according to the SESAME guidelines (SESAME, 2004). To minimize transient disturbances, particularly traffic-related noise, each signal was segmented into 30 s windows using an STA/LTA anti-trigger algorithm. Fourier spectra were then calculated using the Konno and Ohmachi (1998) smoothing procedure, applying a 5% cosine taper, a smoothing constant of 30, and a frequency range of 0.5-40 Hz.

The H/V ratio was computed for each valid window by dividing the average of the two horizontal spectra by the vertical spectrum, and the mean H/V curve was subsequently derived. From this curve, the fundamental resonance frequency (f_0) and its corresponding amplification amplitude (A_0) were identified from the main spectral peak. These parameters constitute key indicators for assessing local site effects and the seismic amplification potential of the studied area.

3.2 MASW

The Multichannel Analysis of Surface Waves (MASW) is a non-invasive geophysical method commonly applied to determine the shear-wave velocity (Vs) structure of shallow subsurface materials by analyzing the dispersion of Rayleigh waves. Since Vs is closely linked to the mechanical stiffness of the ground, low values generally reflect loose, unconsolidated, or fractured materials, whereas high values usually correspond to more competent formations or seismic bedrock (Ayele et al., 2022).

In this study, MASW measurements were conducted along 15 profiles distributed throughout the study area using an ABEM seismograph coupled with 24 vertical geophones of 4.5 Hz natural frequency (Fig. 3). The geophones were deployed in a linear layout with 5 m spacing, resulting in a total spread length of 115 m. A 10 kg sledgehammer striking a metal plate served as the seismic source, positioned 2.5 m from the first geophone to minimize near-field effects and enhance the quality of the recorded surface waves. Data were acquired with a sampling frequency of 2000 Hz, a sampling interval of 1 ms, and a record length of 1 s.

The recorded data were processed with SeisImager software. For each profile, the fundamental-mode Rayleigh-wave dispersion curve was extracted and inverted using a damped least-squares method to derive one-dimensional V_s profiles, allowing assessment of the vertical shear-wave velocity distribution and the stiffness of the subsurface layers.

3.3 SRT

Seismic Refraction Tomography (SRT) is an active seismic method commonly used to image the geometry and physical properties of shallow subsurface formations through the analysis of first-arrival P-wave travel times. Variations in seismic velocity help identify lateral and vertical changes in lithology, degree of compaction, and the depth to competent substratum, while tomographic inversion is particularly well suited to complex near-surface conditions (Reynolds, 2011; Khadrouf et al., 2024).

In this study, SRT data were acquired along 25 profiles distributed across the study area using an ABEM 24-channel seismograph coupled with 24 vertical geophones of 4.5 Hz natural frequency (Fig. 3). The geophones were arranged in a linear array with 5 m spacing, corresponding to a total spread length of 115 m. A 10 kg sledgehammer striking a metallic plate was used as the seismic source. For each profile, five shot points were performed, including two end shots, two intermediate shots, and one central shot. The data were recorded with a sampling interval of 0.5 ms and a record length of 500 ms. First-arrival times were manually picked and processed in SeisImager software. The data were then inverted using an iterative least-squares tomographic algorithm to generate two-dimensional P-wave velocity models, providing valuable information on the shallow subsurface structure.

3.4 DPT/Boreholes

Dynamic probing tests (DPT, Type B) were carried out in accordance with NF P94-115 norm to characterize the spatial variability of near-surface soil stiffness and resistance across the urban area (Fig. 3). For each test, the dynamic cone resistance profile, $q_d(z)$, was reduced to a single representative value to allow geostatistical mapping. Because q_d commonly follows a log-normal distribution and may include high spikes related to very dense layers

or refusal conditions, particularly above limestone, a thickness-weighted geometric mean was adopted as a robust measure of central tendency. In addition, individual q_d values were capped at 500 bar before averaging in order to limit the effect of refusal-controlled outliers and preserve sensitivity to the soil cover.

The representative DPT value at each point, q_d,eq, was converted into an equivalent serviceability bearing pressure, q_{els}, using the relation $q_{els} = q_d$,eq/21. This reduction factor was adopted following the empirical Dutch-L'Herminier approach, in which dynamic cone resistance is converted into an allowable or serviceability bearing pressure using a conservative reduction coefficient commonly close to 20-22 for preliminary shallow foundation assessment (Sanglerat, 1973). The value of 21 was therefore selected as an intermediate conservative value. It should be noted that, in this study, q_{els} is used as a comparative geotechnical indicator for spatial zoning and not as a final design bearing capacity. To improve the statistical behavior of the data before kriging, $\log_{10}(q_{els})$ was interpolated instead of the raw values. The interpolated results were then back-transformed into bar units. This approach provides one comparable geotechnical indicator per test point for spatial interpolation and zoning. In addition, four 10 m deep boreholes were carried out to correlate the DPT results with the local lithological conditions (Fig. 3).

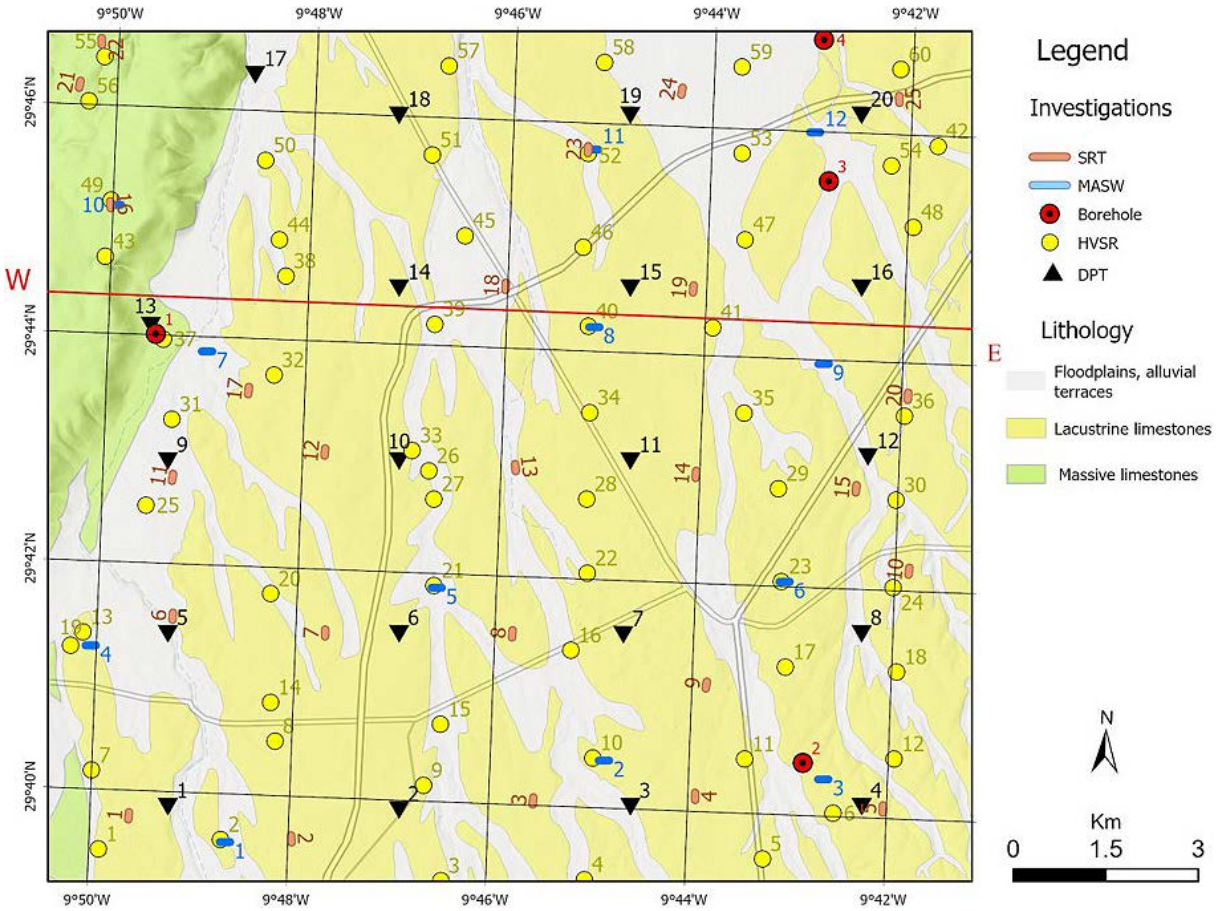

Figure 3. Location of geophysical and in situ investigations within the study area.

4. Results

4.1 Distribution of fundamental frequencies (f_0)

The fundamental frequency (f_0) derived from the 60 HVSR measurements ranged from 1.5 to 18 Hz, indicating some lateral variability across the study area. Despite this range, flat H/V curves dominated the dataset, i.e., many stations did not show a stable, well-defined resonance peak (Fig. 6A).

Representative examples are HVSR-33, HVSR-35, and HVSR-36, which remained close to unity over the investigated band and exhibited consistently low amplitudes. The lowest frequencies (1.5-3 Hz) occurred at only a small number of

sites (Fig. 4) and did not define a clear spatial trend. Their limited occurrence suggests that thicker, softer sedimentary packages capable of producing long-period resonance were localized rather than basin-wide.

Frequencies in the intermediate band (3-8 Hz) were more commonly observed and were mainly distributed around the mapped alluvial corridors and terrace/floodplain sectors (Fig. 6A), consistent with moderate contrasts between unconsolidated cover and the underlying competent substratum.

Higher frequencies (>8 Hz) were also detected at several stations, but again without a continuous spatial gradient (Fig. 4 and Fig. 5). Importantly, only a few sites exhibited clear peaked or multi-peaked HVSR signatures. HVSR-37 and HVSR-31 showed pronounced peaks near the high-frequency end of the plots (around ~18-20 Hz), with additional secondary peaks at lower frequencies, indicating more complex shallow layering or multiple impedance contrasts (Fig. 4). Along the E-W cross-section, the contrast between curve typologies was systematic: flat curves aligned with sectors where the competent limestone appears very shallow, whereas the peaked/multi-peaked responses coincided with localized sedimentary pockets along the profile (Fig. 5).

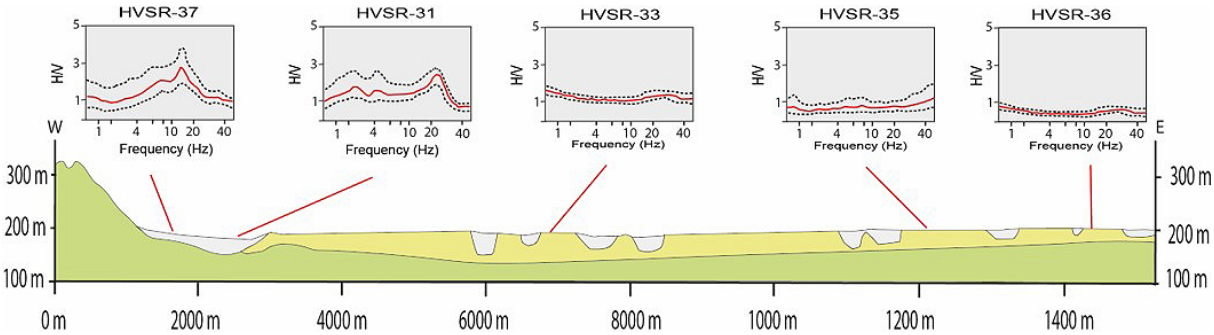

Figure 4. Representative HVSR spectral curves and corresponding geological cross-section in the study area.

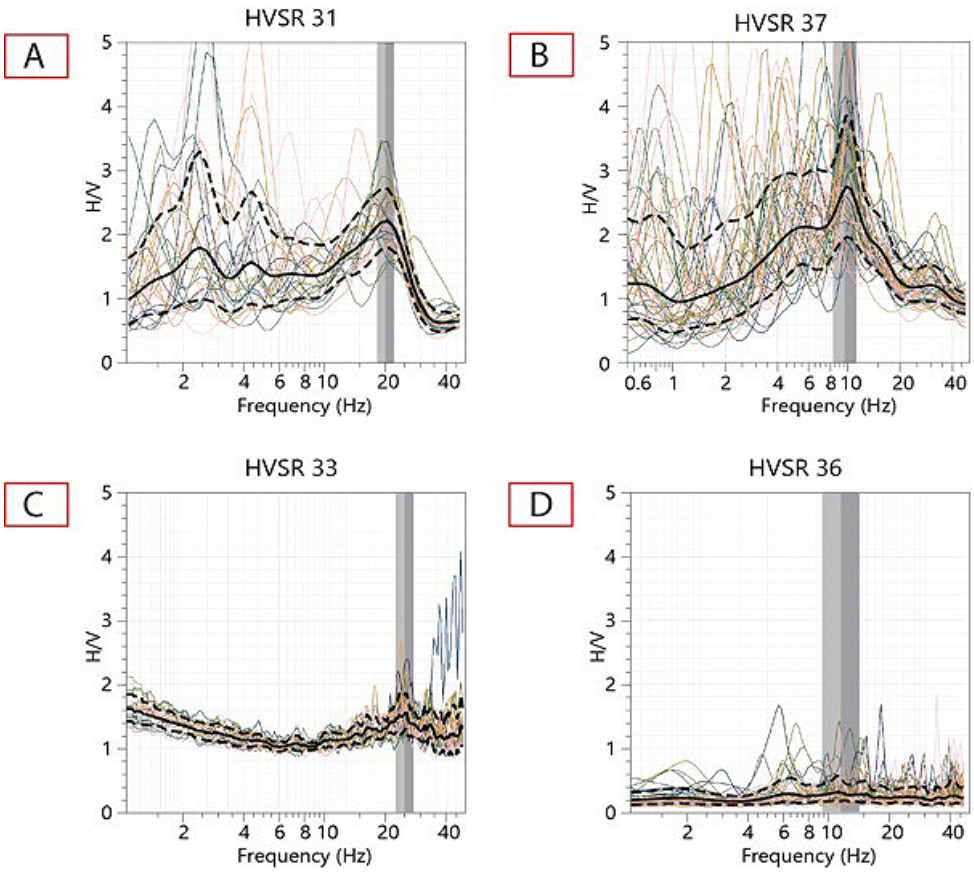

Figure 5. Representative HVSR spectral curves and corresponding geological cross-section in the study area.

4.2 Distribution of the peak amplitude (A_0)

The mapped peak amplitude (A_0) showed generally low-to-moderate amplification, with most non-flat sites falling between approximately $A_0 = 2$ and 3. Many stations were again classified as flat curves, consistent with the prevalence of peak-free HVSR responses observed in the f_0 results (Fig. 6B).

The highest A_0 class (~3) was restricted to a limited number of points, mainly in the southern to southeastern part of the map and a few isolated locations elsewhere (Fig. 6B). Where clear peaks were visible in the representative curves (e.g., HVSR-31 and HVSR-37), amplitudes locally approached the upper end of the mapped range (Fig. 5A and 5B).

Overall, the combined f_0-A_0 patterns indicated that, across most of the area, the near-surface response was characterized by weak resonance (flat curves) and limited amplification, consistent with a shallow competent substratum and/or reduced impedance contrast. In contrast, localized sedimentary pockets produced identifiable resonances (including multi-peaked behavior) and modest A_0 values (Fig. 6B), implying spatially limited site-effect "hotspots" rather than a continuous amplification zone.

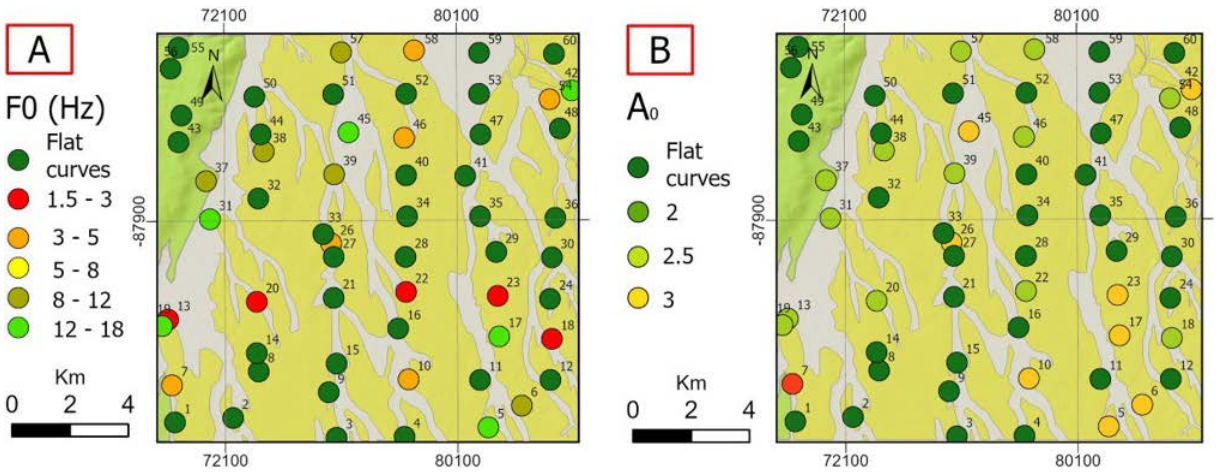

Figure 6. (A) Distribution of the fundamental frequency (f_0); (B) Amplitude of the HVSR peak (A_0) in the study area.

4.3 Seismic basement depth from SRT

The seismic basement depth was mapped by gridding the bedrock picks extracted from all SRT refraction profiles acquired across the study area (Fig. 8A). The basement horizon was consistently defined as the first continuous layer exhibiting high P-wave velocity (Vp > 3.5 km/s), interpreted as competent substratum (bedrock) based on the velocity stratification observed in the individual sections.

The resulting surface highlights a predominantly shallow basement, with depths ranging from <0.5 m to ~3 m. Most of the area is characterized by basement depths ≤1.5 m, indicating limited thickness of unconsolidated to weakly consolidated cover. In contrast, a pronounced bedrock depression is observed along the entire western margin of the study area, where basement depths locally reach ~2-3 m. This elongated deepening closely follows the N-S corridor of Oued Adoudou, indicating a laterally continuous increase in the thickness of unconsolidated to weakly consolidated deposits along the river pathway, likely driven by channel incision and floodplain aggradation. A secondary domain of moderately deeper basement (~1.5-2 m) is also outlined from the south-eastern to central-eastern sector, surrounded by the dominant shallow-bedrock domain.

Overall, the SRT-derived basement geometry is consistent with the local lithological organization: shallow basement corresponds to areas dominated by the lacustrine limestone unit, whereas deeper basement aligns with the alluvial corridor/floodplain where unconsolidated deposits are expected to thicken. This agreement supports the reliability of the SRT interpretation and confirms that near-surface geological facies exert the primary control on basement depth variability at the scale of the investigation.

4.4 Soil Classification based on V_{s30}

The V_{s30} values obtained from MASW profiles range from less than 600 m/s to approximately 860 m/s reflecting generally stiff mechanical conditions in the study area (Figs. 7 and 8B). The average shear-wave velocity in the upper 30 m is commonly used for seismic site characterization and serves as the basis for classification systems such as NEHRP and Eurocode 8.

Lower V_{s30} values (<600 m/s) are mainly concentrated in the western sector. In this area, SRT results indicate basement depths of about 2-3 m (Fig. 7B), and DPT soundings show a progressive increase in dynamic resistance reaching similar depths. These sectors are also associated with relatively low fundamental frequencies (1.5-3 Hz), reflecting a greater sediment thickness and reduced stiffness of the superficial layers.

Higher V_{s30} values (760-860 m/s) are observed predominantly in the northern and southern parts of the site. These zones correspond to shallow basement conditions, generally less than 1 m according to SRT and DPT. Between these two domains, a west-east oriented central belt (600-760 m/s) marks a gradual transition in mechanical properties, indicating a lateral stiffness gradient at the local scale.

According to Eurocode 8, most of the study area falls within soil class B, with V_{s30} between 360 and 800 m/s, while velocities above 800 m/s correspond to class A conditions.

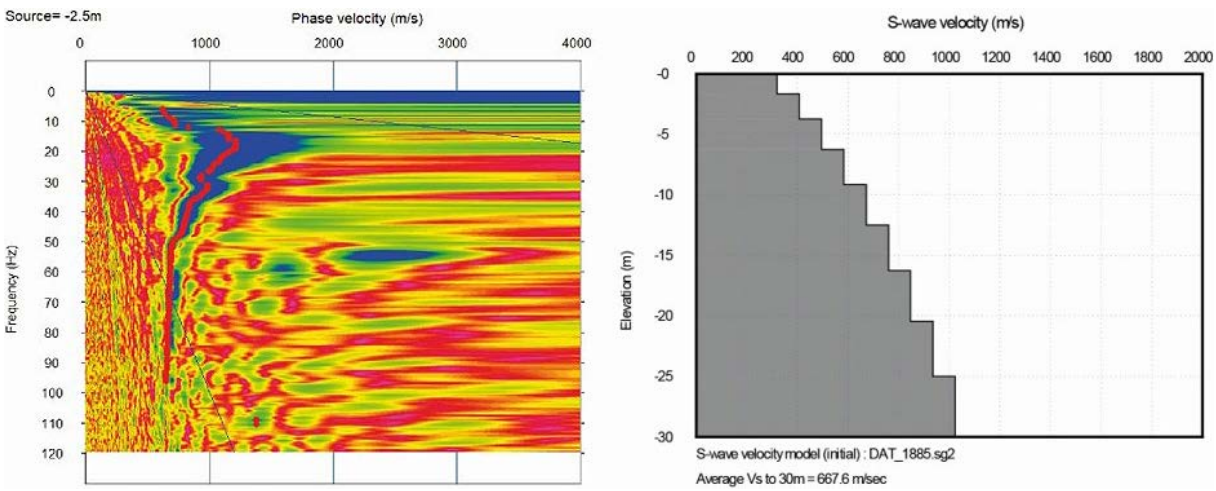

Figure 7. Representative MASW dispersion image and corresponding 1D shear-wave velocity model for profile MASW5.

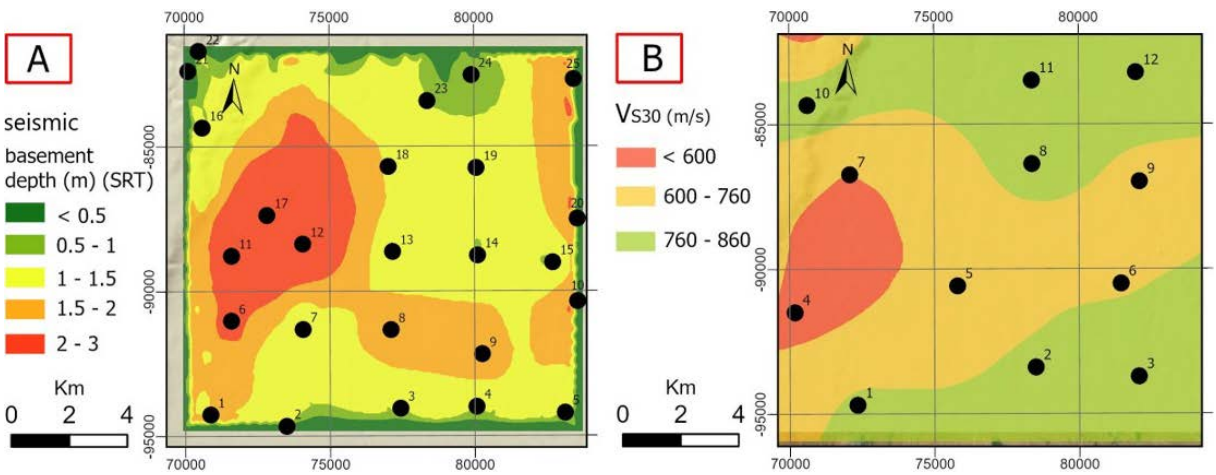

Figure 8. (A) Seismic basement depth from SRT (m); (B) Averaged shear-wave velocity in the top 30 meters (Vs30).

4.5 Geotechnical basement depth from DPT

The geotechnical basement depth obtained from the Dynamic Penetration Tests (DPT) shows that the subsurface conditions in the study area are shallow. The depth varies from less than 0.5 m to about 3 m, which indicates a thin sedimentary cover over a resistant substratum (Fig. 11A).

The greatest basement depths (2-3 m) are observed in the northwestern and southwestern sectors. In these areas, profiles DPT-05 and DPT-17 in the Fig. 8 display a progressive increase in dynamic resistance with depth followed by a marked rise (around 600 bars) marking the transition to the resistant horizon. This behavior reflects the presence of relatively thicker superficial deposits compared to other parts of the site. Borehole BH-04, conducted in the study area, revealed a thick clayey silt deposit underlying the limestone (Fig. 10).

Intermediate basement depths, generally between 1 and 2 m according to the Fig. 4 characterize transitional zones between the thicker sectors and the shallower domains. The DPT-09 and DPT-06 profiles located near these areas, show a faster increase in resistance with depth, reaching values between 700 and 800 bars at approximately 3 m, reflecting moderate sediment thickness and sharper mechanical contrast (Fig. 9).

More superficial conditions dominate the central, northeastern, and southeastern parts of the study area. The profiles DPT-10 and DPT-11 show that high resistance values are reached around 1 m depth, while DPT-01 and DPT-07 record resistance values above 800 bars from the first decimeters. These results confirm that the competent substratum is encountered almost immediately below the surface in these sectors (Fig. 9). The investigated depths are consistent with the borehole lithology, which reveals a shallow basement composed of limestone or schist (Fig. 10).

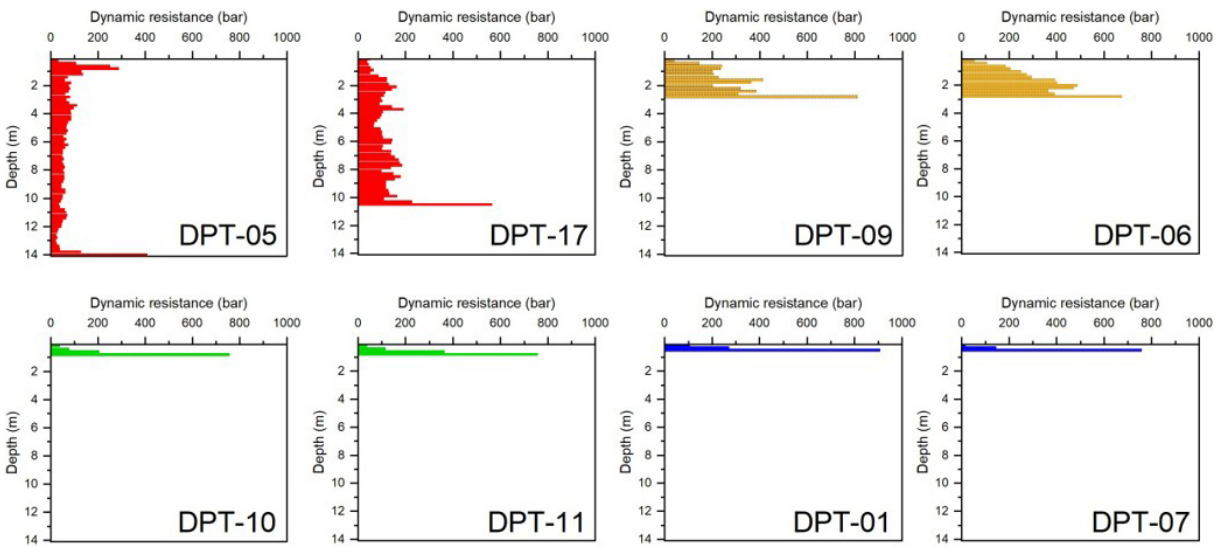

Figure 9. Representative dynamic cone resistance (qd) profiles from selected DPT soundings across the study area.

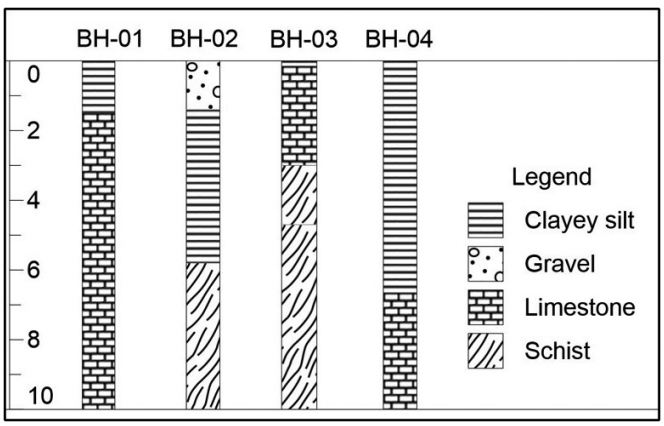

Figure 10. Borehole lithological logs showing the shallow subsurface stratigraphy in the study area.

4.6 Equivalent serviceability bearing pressure (q_{els})

The equivalent serviceability bearing pressure (q_{els}) map obtained from the DPT dataset (Fig. 11B) reveals a marked spatial variability of near-surface serviceability conditions across the urban area. Interpolated q_{els} values range from ~1 to 13 bar, with most of the site falling within the 5-10 bar interval, indicating generally good ground performance under serviceability criteria. The highest q_{els} domain (10-13 bar) is concentrated in the central to south-central sector, extending locally toward the north-central part of the area, which reflects stiffer ground and a reduced sensitivity to settlement for typical shallow foundations.

In contrast, lower q_{els} values (1-5 bar) occur as discontinuous pockets, mainly along the western side and toward the south-eastern margins, suggesting a thicker and/or softer near-surface cover where settlement control becomes more critical. Overall, the map delineates a coherent pattern of higher serviceability capacity in the central domain, providing a practical basis for serviceability-oriented geotechnical zoning and for prioritizing areas requiring site-specific checks or ground improvement.

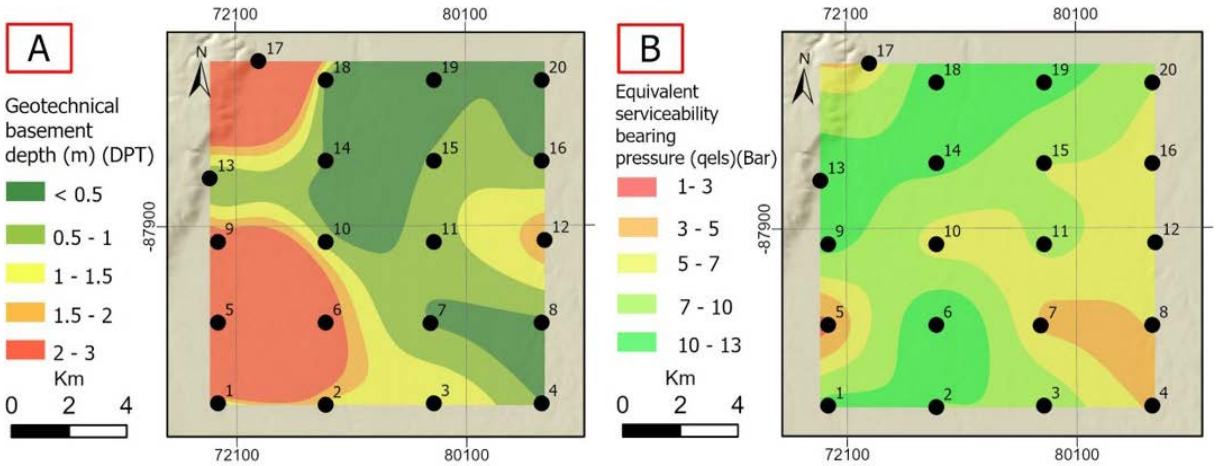

Figure 11. (A) Interpolated maps derived from DPT data showing geotechnical basement depth (m) and (B) equivalent serviceability bearing pressure, q_{els} (Bar), across the study area.

5. Discussion

The integrated results indicate that most of the Tiznit urban extension area is characterized by stiff to very stiff near-surface conditions and a shallow competent horizon. This interpretation is supported by the SRT results, which show a high-velocity layer generally located within the first 0.5-1.5 m and locally deepening to about 2-3 m, and by the DPT data, which indicate a rapid increase in dynamic resistance at shallow depth over large parts of the area. These observations are also consistent with the predominance of flat or weakly peaked HVSR curves and with MASW-derived V_{s30} values mostly corresponding to Eurocode 8 class B, locally reaching class A. Therefore, over most of the investigated area, seismic amplification related to thick soft deposits is expected to be limited. This interpretation is consistent with the use of HVSR as a tool for identifying resonance frequency and impedance contrasts, while considering the limitations of amplitude interpretation (Molnar et al., 2022; Khadrouf et al., 2024).

However, this general shallow-bedrock model does not explain all observations. A small number of HVSR sites show low-frequency responses in the range of 1.5-3 Hz. Such frequencies are not compatible with a simple model consisting only of 2-3 m of superficial soil overlying a rigid layer. For example, assuming an average V_s of 300-400 m/s, a resonance frequency of about 2 Hz would imply an effective contrast depth of roughly 37-50 m using the classical quarter-wavelength relationship. This depth is much greater than the shallow geotechnical horizon detected by DPT and SRT. This suggests that the few low-frequency HVSR sites are probably controlled by a deeper impedance contrast or by a more complex local structure, rather than by the shallow resistant layer alone (Bonnefoy-Claudet et al., 2006; SESAME, 2004).

This distinction is important because the "basement" identified by the different methods does not necessarily have the same physical meaning. The DPT basement corresponds to a mechanically resistant horizon defined by high cone resistance or refusal conditions, while the SRT basement corresponds to a shallow high-P-wave-velocity refractor. In contrast, the HVSR fundamental frequency is controlled by the strongest impedance contrast affecting the ambient vibration wavefield, which may occur at greater depth. Consequently, the few low-frequency HVSR peaks may reflect deeper weathered or clayey units below the shallow limestone, a buried alluvial/colluvial corridor, or a velocity contrast located below the investigation depth of the DPT soundings and only partly constrained by the MASW profiles (Bonnefoy-Claudet et al., 2006; Molnar et al., 2022).

The joint analysis of spatially close HVSR and MASW data provides important constraints on the localized low-frequency responses. In sectors where possible resonance coincides with comparatively lower shear-wave velocities, the observed behavior is more likely related to a deeper or gradual impedance contrast than to the shallow soil cover identified by DPT and SRT alone. The use of MASW-derived Vs profiles to constrain the interpretation of HVSR peaks is therefore essential, because HVSR alone may be affected by non-uniqueness and cannot provide a unique velocity-depth model without additional constraints (Foti et al., 2018).

The DPT and borehole results also support the presence of local heterogeneity. Although most DPT profiles reach high resistance at shallow depth, DPT05 and DPT17 show a more progressive increase in dynamic resistance, indicating thicker or mechanically more gradual superficial deposits. In addition, borehole observations locally show lithological heterogeneity beneath the shallow competent horizon, including clayey-silty levels below limestone. Such configurations may generate complex impedance conditions and may explain why a limited number of HVSR curves show low-frequency or multi-peaked behavior despite the presence of shallow resistant layers. Multi-peaked or broad HVSR curves are commonly associated with layered or laterally heterogeneous subsurface conditions, and their interpretation requires caution (Khadrouf et al., 2024).

From an engineering point of view, the results therefore indicate two different situations. Over most of the area, the shallow competent substratum implies favorable conditions for ordinary shallow foundations, and seismic site amplification is expected to remain minor. In contrast, the few low-frequency HVSR sites should be considered localized zones of potential site-effect sensitivity. These zones do not invalidate the general stiff-ground interpretation of the area, but they indicate that the subsurface structure is locally more complex than suggested by the shallow geological model alone. Consequently, these sectors should be prioritized for additional project-scale investigations, especially where important buildings, sensitive infrastructure, or deeper excavations are planned.

Overall, the microzonation significance of this study lies not in identifying a broad amplification-prone basin, but in distinguishing a dominant stiff-ground domain from a limited number of localized sectors where deeper impedance contrasts or heterogeneous deposits may produce measurable resonance. This refined interpretation provides a more realistic basis for urban planning in Tiznit: most of the area appears favorable from a seismic site-response perspective, while the low-frequency HVSR sectors require more detailed 1D modeling and local geotechnical verification before final design decisions.

6. Conclusion

This study demonstrates that the Tiznit urban extension area is not characterized by a continuous soft sedimentary basin, but by a predominantly stiff and shallow-bedrock setting, locally interrupted by discrete sectors of weaker near-surface conditions. The integrated interpretation of HVSR, MASW, SRT, DPT, boreholes, and geological observations shows that most of the area is underlain by a competent substratum encountered at shallow depth, generally within 0.5-1.5 m and only locally deepening to about 2-3 m, especially along the western corridor associated with Oued Adoudou. This geometry is consistent with the seismic response pattern: HVSR curves are mostly flat or weakly peaked, peak amplitudes are generally low to moderate, and only a few sites display clear or multi-peaked resonances, indicating that impedance contrasts are limited over most of the study area and become significant only in localized heterogeneous pockets.

The MASW results further support this interpretation by indicating generally high shallow stiffness, with V_{s30} values ranging from less than 600 m/s to about 860 m/s and a predominance of Eurocode 8 class B conditions, locally reaching class A. In parallel, the DPT-derived geotechnical parameters confirm that favorable serviceability conditions dominate much of the site, with most q_{els} values falling between 5 and 10 bar, while lower-capacity sectors are confined mainly to the western and southeastern margins. Taken together, these results show that the

principal engineering issue in Tiznit is not widespread seismic amplification, but rather the identification and management of localized zones where thicker superficial deposits, lower stiffness, deeper bedrock, and reduced bearing capacity coincide.

From a microzonation perspective, the main contribution of this work is therefore to replace generalized code-based assumptions with a site-specific and spatially resolved characterization of ground behavior. The study shows that V_{s30} alone would not fully capture the observed variability, and that reliable zoning in Tiznit requires the joint consideration of resonance characteristics, shallow velocity structure, seismic and geotechnical basement geometry, and serviceability resistance. This integrated framework provides a practical basis for urban planning, preliminary foundation assessment, and the prioritization of areas requiring additional investigation or possible ground improvement. The engineering implications are expected to be more significant for lightweight structures and shallow infrastructures, whereas critical or heavily loaded structures still require detailed site-specific investigations.

However, because local heterogeneity remains significant at the project scale, the proposed zoning should be regarded as a planning and screening tool rather than a substitute for detailed site investigations prior to the design of critical, sensitive, or heavily loaded structures.

Future investigations should focus on converting the derived seismic proxies into engineering-oriented design spectra and amplification factors suitable for structural applications. Additional work is also needed to explicitly quantify uncertainty related to lateral heterogeneity and inversion non-uniqueness and to propagate these effects into microzonation products. Furthermore, higher-density boreholes and geotechnical investigations are recommended in the western sector and other localized heterogeneous zones to improve site-scale characterization.

Data availability statement. All relevant data are provided in the supplementary file accompanying this manuscript

Acknowledgements. The authors thank the Editor in Chief, and reviewers for their time and constructive comments towards improving our manuscript.

References

Ayele, A., K. Woldearegay and M. Meten (2022). Multichannel Analysis of Surface Waves (MASW) to estimate the shear wave velocity for engineering characterization of soils at Hawassa Town, Southern Ethiopia, Int. J. Geophys., 2022, 1-22, doi:10.1155/2022/7588306.

Bonnefoy-Claudet, S., F. Cotton and P. Y. Bard (2006). The nature of noise wavefield and its applications for site effects studies: A literature review, Earth Sci. Rev., 79, 3-4, 205-227, doi:10.1016/j.earscirev.2006.07.004.

Chaaraoui, A., M. Chourak, M. Hamdache, J. A. Peláez et al. (2022). Amplification analysis at Nador city and surrounding area (NE of Morocco), J. Afr. Earth Sci., 196, 104717, doi:10.1016/j.jafrearsci.2022.104717.

Cherki, F., M. Tadili, B. Tadili and N. Mhammdi (2025). V_{s30} mapping and soil classification in Tiznit region based on H/V spectral ratio method, E3S Web Conf., 607, 04004, doi:10.1051/e3sconf/202560704004.

El Hilali, M., A. Bounab, Y. Timoulali, J. Messari et al. (2023). Seismic site-effects assessment in a fluvial sedimentary environment: case of Oued Martil floodplain, Northern Morocco, Nat. Hazards, 1-23, doi:10.1007/s11069-023-06032-8.

Essaied, A., M. Rouai and K. Bouhali (2025). Microzonation and classification of seismic sites based on analysis and modeling of the HVSR data in the city of Meknes, Morocco, Soil Dyn. Earthq. Eng., 196, 109451, doi:10.1016/j.soildyn.2025.109451.

Foti, S., F. Hollender, F. Garofalo, D. Albarello et al. (2018). Guidelines for the good practice of surface wave analysis: a product of the InterPACIFIC project, Bull. Earthq. Eng., 16, 6, 2367-2420, doi:10.1007/s10518-017-0206-7.

Hitouri, S., E. A. Toto, M. Hafid, A. Ibenbrahim et al. (2025). Seismic site effects and aptitude to urbanization for the study area of Taroudant, South-West of Morocco, J. Appl. Geophys., 241, 105856, doi:10.1016/j.jappgeo.2025.105856.

Khadrouf, I., O. El Hammoumi, N. El Goumi and M. Oukassou (2024). Contribution of HVSR, MASW, and geotechnical investigations in seismic microzonation for safe urban extension: A case study in Ghabt Admin (Agadir), western Morocco, J. Afr. Earth Sci., 210, 105138, doi:10.1016/j.jafrearsci.2023.105138.

Khadrouf, I., O. El Hammoumi, N. El Goumi, A. El Atillah et al. (2024). Enhancing geotechnical zoning through near-surface geophysical surveys: a case study from eastern Agadir, Morocco, Mediterr. Geosci. Rev., 6, 3, 233-248, doi:10.1007/s42990-024-00137-3.

Khadrouf, I., M. El Hilali, N. El Goumi, O. El Hammoumi et al. (2026). Enhancing wind farm site characterization using multi-geophysical approaches for high-resolution subsurface imaging in Midelt, Central Morocco, J. Appl. Geophys., 250, 106277, doi:10.1016/j.jappgeo.2026.106277.

Konno, K. and T. Ohmachi (1998). Ground-motion characteristics estimated from spectral ratio between horizontal and vertical components of microtremor, Bull. Seismol. Soc. Am., 88, 1, 228-241, doi:10.1785/BSSA0880010228.

Lamine, S., A. Najine, H. Lemacha, W. Lachhab et al. (2026). Seismic characterization of the Western Sidi Ifni region (Morocco): insights from surface wave and ambient vibration methods, Mediterr. Geosci. Rev., 8, 1, 275-291, doi:10.1007/s42990-026-00223-8.

Molnar, S., A. Sirohey, J. Assaf, P. Y. Bard et al. (2022). A review of the microtremor horizontal-to-vertical spectral ratio (MHVSR) method, J. Seismol., 26, 4, 653-685, doi:10.1007/s10950-021-10062-9.

Nakamura, Y. (1989). A method for dynamic characteristics estimation of subsurface using microtremor on the ground surface, Q. Rep. Railway Tech. Res. Inst., 30, 1.

NF P94-115 (n.d.). Soils: investigation and testing – in situ tests – dynamic penetration B-type test, AFNOR, Paris.

Nogoshi, M. and T. Igarashi (1970). On the propagation characteristics of microtremors, J. Seismol. Soc. Jpn., 23, 264-280.

Nouayti, A., L. E. Moudnib, D. Khattach, M. Zeckra et al. (2024). Seismic synthesis of the Al Haouz earthquake of September 8th, 2023 by integrating gravimetric and aeromagnetic data from the western High Atlas in Morocco, Model. Earth Syst. Environ., 10, 6, 6639-6658, doi:10.1007/s40808-024-02148-3.

Reynolds, J. M. (2011). An introduction to applied and environmental geophysics, John Wiley & Sons, Chichester.

RPS (2011). Le règlement de construction parasismique RPS 2000, version 2011, Ministère de l'Habitat et de la Politique de la Ville, Rabat, Morocco.

Sanglerat, G. (1972). The penetrometer and soil exploration, Elsevier, Amsterdam.

Sehrt, M. (2014). Variscan to Neogene long-term landscape evolution at the Moroccan passive continental margin (Tarfaya Basin and western Anti-Atlas), PhD Thesis, Heidelberg University, Heidelberg.

SESAME (2004). Guidelines for the implementation of the H/V spectral ratio technique on ambient vibrations: measurements, processing and interpretation, SESAME European Research Project, 62.

Soulaimani, A. and M. Bouabdelli (2005). Le Plateau de Lakhssas (Anti-Atlas occidental, Maroc): un graben fini-précambrien réactivé à l'Hercynien, Ann. Soc. Géol. Nord, 12, 177-184, doi:10.3406/asgn.2005.2271.

Wanaim, A., M. A. Belfoul, S. Bouzid and F. Faik (2014). Speleogenesis and evidences tectonic into Lakhssas Karst System (Western Anti-Atlas, Morocco), Open J. Geol., 4, 7, 314-323, doi:10.4236/ojg.2014.47024.

Wathelet, M., J. L. Chatelain, C. Cornou, G. Di Giulio et al. (2020). Geopsy: A user-friendly open-source tool set for ambient vibration processing, Seismol. Res. Lett., 91, 3, 1878-1889, doi:10.1785/0220190360.

****CORRESPONDING AUTHOR: Ismaail KHADROUF**,
Hassan II University of Casablanca, Faculty of Sciences Ben M'sick,
Laboratory of Geosciences, Geomatics and Environment, Morocco
e-mail: ismaail.khadrouf-etu@etu.univh2c.ma

© 2026 the Author(s).
Open Access. This article is licensed under a Creative Commons Attribution 4.0 International License